Electro-optic millimeter-wave harmonic downconversion and vector demodulation using cascaded phase modulation and optical filtering

Vincent R. Pagán[1,2,*] and Thomas E. Murphy[1,2,3]

[1]*Laboratory for Physical Sciences, College Park, Maryland 20740, USA*

[2]*Department of Electrical & Computer Engineering, University of Maryland, College Park, Maryland 20742, USA*

[3]*Institute for Research in Electronics and Applied Physics, University of Maryland, College Park, Maryland 20742, USA*

**Corresponding author: vrpagan@lps.umd.edu*

Received March 23, 2015; accepted April 9, 2015;
posted April 28, 2015 (Doc. ID 235035); published May 19, 2015

We describe and demonstrate an electro-optic technique to simultaneously downconvert and demodulate vector-modulated millimeter-wave signals. The system uses electro-optic phase modulation and optical filtering to perform harmonic downconversion of the RF signal to an intermediate frequency (IF) or to baseband. We demonstrate downconversion of RF signals between 7 and 70-GHz to IFs below 20-GHz. Furthermore, we show harmonic downconversion and vector demodulation of 2.5-Gb/s QPSK and 5-Gb/s 16-QAM signals at carrier frequencies of 40-GHz to baseband. © 2015 Optical Society of America

OCIS codes: (060.5625) Radio frequency photonics; (060.2360) Fiber optics links and subsystems; (060.5060) Phase modulation; (060.3735) Fiber Bragg gratings.

http://dx.doi.org/10.1364/OL.40.002481

Frequency downconversion is an essential process in millimeter-wave (mmW) receivers that translates a received RF signal to a lower intermediate-frequency (IF) or baseband signal that can be more easily detected, demodulated, or digitized. Traditional frequency downconverters employ electrical mixers, but electro-optic downconversion systems offer compelling advantages, especially for wide bandwidth signals at microwave and millimeter-wave frequencies. By imparting the RF signal and electrical local oscillator (LO) onto an optical carrier, it is possible to take advantage of the wider bandwidth, lower loss, electromagnetic isolation, and smaller size and weight of fiber optic components.

Several electro-optic downconversion approaches have been reported in the literature, based upon sequential or parallel intensity modulators [1–7] or phase modulators [8–10]. Systems employing phase modulation have the advantage that they do not need bias control circuitry, but they require a dispersive, interferometric or frequency-selective element to convert the phase modulation into a signal that can be directly detected [11–13]. In intensity modulated systems, the $\cos^2(\cdot)$ nonlinear transfer function allows one to employ a harmonic of the LO to downconvert higher frequencies, which greatly reduces the cost and complexity of the system [14,15].

While most prior electro-optic downconversion systems provide only a single quadrature, simultaneous downconversion of both the in-phase (I) and quadrature (Q) components makes it possible to measure the relative phase of the incoming RF signal and has applications including direction finding, directional tracking, heterodyne image rejection, and demodulation of vector modulated signals [16,17].

In this Letter, we describe a simple electro-optic I/Q downconverter that uses cascaded phase modulation followed by optical notch filtering. We show that the strong Bessel-function nonlinearity of the phase modulator and filter enables efficient harmonic downconversion at up to 4× the LO frequency, allowing for broadband, reconfigurable downconversion of signals ranging from 7 to 70 GHz. We use the system to experimentally demonstrate fourth-order harmonic downconversion and I/Q vector demodulation of QPSK and 16-QAM encoded mmW signals at a carrier frequency of 40 GHz and data-rates of up to 5-Gb/s.

Figure 1 is a simplified schematic of the electro-optic system used for harmonic downconversion of one quadrature, which is a generalized version of the system considered in [8]. A continuous-wave laser with frequency $\omega = 2\pi c/\lambda$ and power P is phase modulated by a mmW signal, $v(t) = V \sin \Omega t$, to produce an optical field given by

$$u_B(t) = \sqrt{P} e^{j\omega t} e^{jm \sin \Omega t}, \tag{1}$$

where $m \equiv \pi V/V_\pi$ is the input signal modulation depth expressed in radians, and V_π is the half-wave voltage of the phase modulator. The second phase modulator is driven by a strong microwave local oscillator, $v(t) = V_0 \sin \Omega_0 t$, to give

$$u_C(t) = \sqrt{P} e^{j\omega t} e^{j(m \sin \Omega t + m_0 \sin \Omega_0 t)} \tag{2}$$

$$= \sqrt{P} e^{j\omega t} \sum_p \sum_q J_p(m) J_q(m_0) e^{j(p\Omega + q\Omega_0)t}, \tag{3}$$

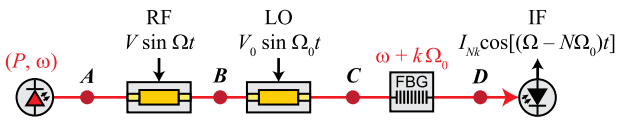

Fig. 1. Schematic of the electro-optic downconverter presented here. The system uses sequential electro-optic phase modulators followed by an optical notch filter and a square-law photodetector.

where $m_0 \equiv \pi V_0/V_\pi$ denotes the modulation depth of the LO and both summations in Eq. (3) are taken to run from $-\Omega$ to $+\Omega$. The RF angular frequency, Ω, is assumed to be close to the Nth harmonic of the LO angular frequency, $N\Omega_0 \simeq \Omega$, in order to downconvert to an intermediate frequency of $\Omega_{\mathrm{IF}} = |\Omega - N\Omega_0|$.

The phase modulated signal is then transmitted through a fiber Bragg grating (FBG) that blocks the kth modulation sideband of the LO, i.e., the reflection band of the FBG is centered at $\omega + k\Omega_0$. This notch filter can be mathematically modeled by excluding from the summation those terms for which $Np + q = k$, where N is the harmonic number, and k denotes the notch filter position. Applying this constraint yields

$$u_D(t) = \sqrt{P}e^{j\omega t}\sum_{\substack{p \\ Np+q\neq k}}\sum_{q} J_p(m)J_q(m_0)e^{j(p\Omega+q\Omega_0)t}. \tag{4}$$

Following the FBG, the optical field is incident on a square-law photodetector having responsivity $\mathcal{R}$ to produce a photocurrent $i(t) = \mathcal{R}|u_D(t)|^2$,

$$i(t) = \mathcal{R}P\sum_{\substack{p \\ Np+q\neq k, Nr+s\neq k}}\sum_{q}\sum_{r}\sum_{s}[J_p(m)J_q(m_0)J_r(m)J_s(m_0) \times e^{j[(p-r)\Omega+(q-s)\Omega_0]t}]. \tag{5}$$

To determine the harmonic downconversion gain of the system, we Taylor expand Eq. (5) to first order in m, and retain only the terms that are oscillating at the downconverted intermediate frequency $\Omega_{\mathrm{IF}} \equiv |\Omega - N\Omega_0|$. This is equivalent to including only the terms in the summation for which $(p - r) = \pm 1$ and $(q - s) \mp N$. With these assumptions, the IF photocurrent simplifies to

$$i_{\mathrm{IF}}(t) = m\mathcal{R}P\eta_{Nk}(m_0)\cos[(\Omega - N\Omega_0)t], \tag{6}$$

where we have introduced the dimensionless downconversion factor $\eta_{Nk}(m_0)$ that depends on the harmonic number N, notch filter position k, and LO modulation depth m_0. Table 1 lists η_{Nk} for several combinations of N and k, as well as the optimal value of m_0 that maximizes the downconversion factor in each case. For downconversion using an odd harmonic, the most efficient combination is generally $k = 0$, which corresponds to suppression of the optical carrier. Even-order harmonics, by contrast, require $k \neq 0$, with $k = 1$ being the most experimentally convenient condition.

Table 1. Downconversion Factor $\eta_{Nk}(m_0)$ for $N \in \{1,2,3,4\}$ and $k \in \{0,1\}$[a]

N	k	η_{Nk}	$m_0^{(\mathrm{opt})}$	$20\log_{10}\lvert\eta_{Nk}^{(\mathrm{opt})}/\eta_{10}^{(\mathrm{opt})}\rvert$
1	0	$2J_0J_1$	1.08	0 dB
2	1	$J_1J_3 + J_1^2$	2.02	–4.4 dB
3	0	$2J_0J_3$	3.95	–5.9 dB
4	1	$J_1J_3 + J_1J_5$	5.19	–10.2 dB

[a]All Bessel functions are assumed to have an argument of m_0. $m_0^{(\mathrm{opt})}$ denotes the LO modulation depth that maximizes the η_{Nk}. The final column compares the downconversion gain to the case of $(N,k) = (1,0)$. Relaxing the constraints on k can yield additional solutions that are not tabulated here.

The net RF-to-IF downconversion gain is then expressed as

$$G_{Nk} = \left(\frac{\pi\mathcal{R}P}{V_\pi}\right)^2 Z_{\mathrm{in}}Z_{\mathrm{out}}\eta_{Nk}^2(m_0), \tag{7}$$

where Z_{in} denotes the input impedance of the signal phase modulator, and the IF photocurrent is applied to an output load impedance of Z_{out}. Here we note that the power P appearing in Eqs. (4)–(7) must be adjusted to account for any gain produced by optical amplification (not shown in Fig. 1) or any optical losses incurred in the phase modulators and filters.

Figure 2 is an experimental diagram showing how the single quadrature system of Fig. 1 was extended to downconvert both quadratures. Following the first RF phase-modulator, the signal is split into two parallel channels that are separately demodulated by two synchronized and appropriately phased local oscillators.

A tunable C-band continuous-wave laser with nominal output power of $P = 16$ dBm was used as the optical source. The RF phase modulator was a 65-GHz, z-cut $LiNbO_3$ phase modulator with measured V_πs of 5.8 V, 6.3 V and 7.6 V at 20-GHz, 40-GHz and 60-GHz, respectively, and an optical insertion loss of 3.4 dB. A nonpolarizing 50/50 optical fiber coupler was used to split the output of the phase modulator into two parallel signals that were used to simultaneously detect I and Q.

In the in-phase arm, a 40-GHz, z-cut $LiNbO_3$ modulator with measured V_πs of 5.1 V, 5.9 V, and 6.7 V at 10-GHz, 20-GHz and 40-GHz, respectively, and an optical insertion loss of 2.5 dB was driven by an electrical LO. The output of the I phase modulator was sent into an athermally packaged fiber Bragg grating having a center wavelength of $\lambda_{\mathrm{FBG}} = 1552.552$ nm. The 3-dB transmission bandwidth of the FBG was measured to be approximately 9.5-GHz, and its out-of-band insertion loss was measured to be approximately 1.6 dB. In transmission, the FBG provided in-band suppression of up to 13 dB relative to its out-of-band insertion loss.

The optical signal transmitted by the FBG was sent through a optical variable delay line that was used to correct the skew between the I and Q channels caused by mismatch in fiber path lengths. The optical signal was then sent into an erbium-doped fiber amplifier (EDFA) operating in constant current mode, followed by a bandpass filter to suppress the amplified spontaneous emission. The post-EDFA bandpass filter does not significantly alter the spectrum of the amplified optical signal. Finally, the optical signal was detected with a PIN photodiode having a bandwidth of 22.3-GHz and a responsivity of $\mathcal{R} = 0.75$ A/W. The components used in the Q arm were nominally identical to those used in the I arm with the exception that $\lambda_{\mathrm{FBG}} = 1552.490$ nm.

To quantify the harmonic downconversion performance, we used a fixed LO frequency of f_0 =20-GHz and swept the input RF frequency, f, from 7 to 70-GHz while measuring the downconverted IF power (in one quadrature) at $f_{\mathrm{IF}} = |f - Nf_0|$, using an electrical spectrum analyzer. Figure 3 shows the measured RF-to-IF downconverted IF power curves as functions of input frequency corresponding to $(N,k) = \{(1,0),(2,1),(3,0)\}$. The LO power was set according to Table 1 to optimize

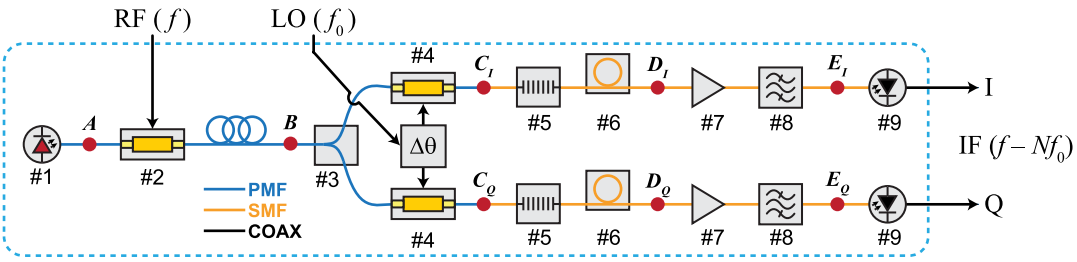

Fig. 2. Simplified schematic of the harmonic downconversion and vector demodulation experimental setup. #1: laser; #2: 65-GHz phase modulator; #3: 50/50 beam splitter; #4: 40-GHz phase modulator; #5: fiber Bragg grating; #6: variable delay line; #7: erbium-doped fiber amplifier; #8: optical bandpass filter; #9: photodetector. The phase difference between the LOs driving the upper and lower 40-GHz phase modulators (#4) was adjusted to satisfy the condition: $\Delta\theta = 90°/N$.

the downconversion factor for each case. Instead of tuning the center frequency of the FBG, the laser was tuned so that either the carrier ($k = 0$) or first sideband ($k = 1$) was suppressed, again in accordance with Table 1. The RF modulation depth was maintained at $m = 0.1$ rad over the full RF-frequency measurement range. The IF bandwidth was primarily limited by the speed of the photodetector.

To demonstrate the vector demodulation capability, we utilized the system to perform baseband demodulation of 40-GHz quadrature phase-shift keyed (QPSK) and quadrature amplitude-modulated (QAM) signals. The vector-modulated signals were produced by a two-channel, 12 GSa/s arbitrary waveform generator (AWG), configured to generate either a 2.5-Gb/s QPSK or a 5-Gb/s 16-QAM signal at an intermediate frequency of 5-GHz. The 5-GHz I and Q outputs from the AWG were combined using a 90° electrical hybrid and upconverted to 40-GHz by mixing with a 35-GHz LO. The resulting data-encoded 40-GHz signal was high-pass filtered, amplified, and applied to the first electro-optic modulator as the RF input.

For fundamental ($N = 1$) vector demodulation, the LO frequency was set to 40-GHz in order to produce baseband I and Q signals. The laser carrier frequency was tuned to the center of the FBGs ($k = 0$), and the LO power was adjusted to achieve $m_0 = 1.08$ in both modulators. Figure 4(a) shows the optical spectrum measured before and after the FBG. The approximate position and notch-width of the FBG are indicated by the highlighted regions. The I and Q channels were amplified and simultaneously recorded on a 1-GHz digitizing oscilloscope. The sample rate of the oscilloscope was set to 1.25 GSa/s, to match the symbol rate of the data pattern.

Figures 5(a) and 5(b) shows the constellation diagrams obtained by plotting a two-dimensional color histogram of the sampled values of I and Q. Both the 2.5-Gb/s QPSK and 5-Gb/s 16-QAM constellations are clearly resolved.

For harmonic demodulation, the LO frequency was set to 10-GHz ($N = 4$), and the laser was de-tuned by 10-GHz, so that the $k = 1$ LO sideband was suppressed by the FBGs, and the LO powers were increased to achieve $m_0 = 5.19$. Figure 4(b) shows the measured optical spectra before and after the FBG with the position of the optical notch filter highlighted. The phase difference between the I and Q LOs was set to 22.5°, in order to produce a 90° difference at 4× the LO frequency ($N = 4$).

Figures 5(c) and 5(d) shows the measured constellation diagrams obtained from $N = 4$ harmonic vector demodulation, for both 2.5-Gb/s QPSK and 5-Gb/s 16-QAM signals, demonstrating successful baseband harmonic demodulation.

In summary, we described a technique to perform harmonic frequency downconversion and phase detection of microwave and mmW signals using phase modulation and optical filtering. Since this configuration utilizes phase modulation, the requirement for bias control

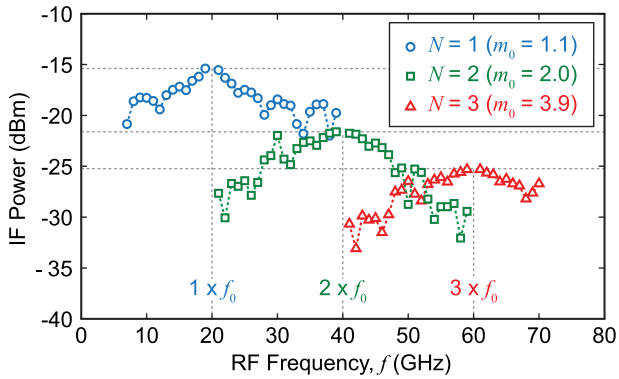

Fig. 3. Intermediate frequency (IF) output power versus RF frequency with a LO frequency of f_0 =20-GHz and an RF modulation depth maintained at $m = 0.1$ rad. The LO modulation depth was set to achieve near-optimal harmonic downconversion gain for $N \in \{1, 2, 3\}$, according to Table 1.

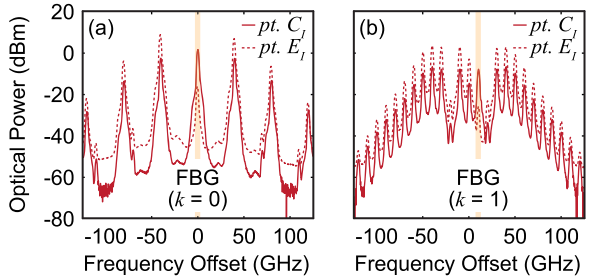

Fig. 4. Optical spectra at points C_I and E_I as referenced to Fig. 3 for (a) $(N, k) = (1, 0)$ and (b) $(N, k) = (4, 1)$. The optical spectra were nominally identical at points C_Q and E_Q and are not shown for clarity. The input RF signal was a 2.5-Gb/s QPSK-encoded mmW signal at f =40-GHz. The LO modulation depths were $m_0 \approx 1.1$ and $m_0 \approx 5.2$ for harmonic downconversion numbers $N = 1$ and $N = 4$, respectively.

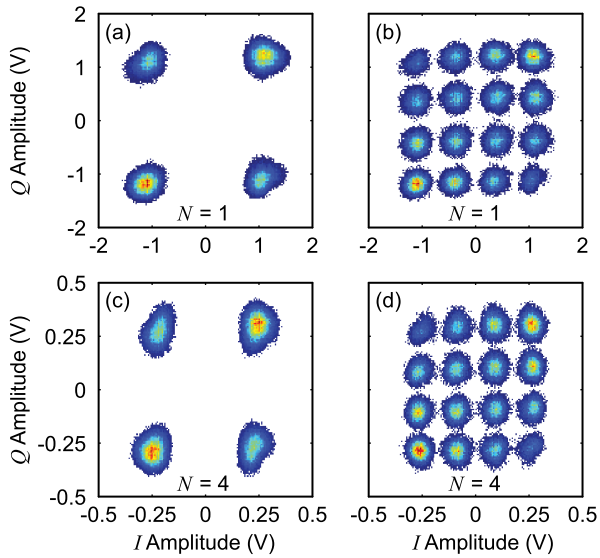

Fig. 5. Baseband constellation diagram histograms (128×128 bins). (a) 2.5-Gb/s QPSK for $(N, k) = (1, 0)$, (b) 5-Gb/s 16-QAM for $(N, k) = (1, 0)$, (c) 2.5-Gb/s QPSK for $(N, k) = (4, 1)$, and (d) 5-Gb/s 16-QAM for $(N, k) = (4, 1)$. The RF carrier frequency was $f = 40$ GHz in all cases.

electronics at each modulator is eliminated. With this approach, we showed that the system is reconfigurable by demonstrating harmonic downconversion of RF signals between 7 and 70-GHz to IFs below 20-GHz using a fixed 20-GHz microwave LO. We further extended this technique to simultaneously downconvert and demodulate vector-modulated mmW signals and experimentally showed harmonic downconversion and vector demodulation of 2.5-Gb/s QPSK and 5-Gb/s 16-QAM signals at carrier frequencies of 40-GHz.

References

1. G. K. Gopalakrishnan, W. K. Burns, and C. H. Bulmer, IEEE Trans. Microwave Theory Technol. **41**, 2383 (1993).
2. X. Gu, S. Pan, Z. Tang, D. Zhu, R. Guo, and Y. Zhao, Opt. Lett. **38**, 2237 (2013).
3. A. Altaqui, E. H. W. Chan, and R. A. Minasian, Appl. Opt. **53**, 3687 (2014).
4. D. Zou, X. Zheng, S. Li, H. Zhang, and B. Zhou, Opt. Lett. **39**, 3954 (2014).
5. Y. Gao, A. Wen, H. Zhang, S. Xiang, H. Zhang, L. Zhao, and L. Shang, Opt. Commun. **321**, 11 (2014).
6. E. H. W. Chan and R. Minasian, J. Lightwave Technol. **30**, 3580 (2012).
7. A. Karim and J. Devenport, J. Lightwave Technol. **26**, 2718 (2008).
8. V. R. Pagán, B. M. Haas, and T. E. Murphy, Opt. Express **19**, 883 (2011).
9. X. Xue, X. Zheng, H. Zhang, and B. Zhou, Opt. Lett. **37**, 1451 (2012).
10. Y. Zhao, X. Pang, L. Deng, X. Yu, X. Zheng, and I. T. Monroy, IEEE Photon. Technol. Lett. **24**, 16 (2012).
11. V. J. Urick, F. Bucholtz, P. S. Devgan, J. D. McKinney, and K. J. Williams, IEEE Trans. Microwave Theory Technol. **55**, 1978 (2007).
12. H. Chi, X. Zou, and J. Yao, J. Lightwave Technol. **27**, 511 (2009).
13. G. Qi, J. Yao, J. Seregelyi, S. Paquet, and C. Bélisle, J. Lightwave Technol. **23**, 2687 (2005).
14. C. K. Sun, R. J. Orazi, S. A. Pappert, and W. K. Burns, IEEE Photon. Technol. Lett. **8**, 1166 (1996).
15. J. Liao, X. Zheng, S. Li, H. Zhang, and B. Zhou, Opt. Lett. **39**, 6565 (2014).
16. P. D. Biernacki, L. T. Nichols, D. G. Enders, K. J. Williams, and R. D. Esman, IEEE Trans. Microwave Theory Technol. **46**, 1784 (1998).
17. R. Sambaraju, J. Palaci, R. Alemany, V. Polo, and J. L. Corral, in *Proceedings of IEEE International Topical Meeting on Microwave Photonics* (IEEE, 2008), pp. 117–120.